12

Crystallization of Frustrated Alkyl Groups in Polymeric Systems Containing Octadecylmethacrylate

Elke Hempel[1], Hendrik Budde[2,3], Siegfried Höring[2], and Mario Beiner[1]

[1] FB Physik, Martin-Luther-Universität Halle-Wittenberg, D-06099 Halle, Germany
beiner@physik.uni-halle.de
[2] FB Chemie, Martin-Luther-Universität Halle-Wittenberg, D-06099 Halle, Germany
[3] Fraunhofer Pilotanlagenzentrum für Polymersynthese und -verarbeitung, Value Park, Bau A74, D-06258 Schkopau, Germany

Abstract. This chapter deals with the crystallization behavior of long frustrated alkyl groups as part of side chain polymers. Results from crystallization experiments on poly(n-octadecylmethacrylate) [PODMA] homopolymers with different molecular weight and on microphase-separated poly(styrene−*block*−octadecylmethacrylate) block copolymers [P(S−*b*−ODMA] by calorimetry and scattering techniques are presented. A phenomenological picture describing the different stages of the side chain crystallization in PODMA is given. The influence of additional constraints in P(S−*b*−ODMA) block copolymers containing PODMA lamellae or cylinders in a glassy environment is studied. It is shown that these block copolymers are systems with a hierarchy of length scales in the nanometer range. The crystallization behavior in PODMA lamellae is basically bulk-like while strong confinement effects are indicated in case of PODMA cylinders with a diameter <20 nm by increasing crystallization times and broader transformation intervals in isothermal crystallization curves. These effects can be explained by changes concerning nucleation mechanism and crystal growth. The reduced degree of crystallinity in small cylinders is discussed based on hypothetical pictures for the internal structure of the PODMA domains.

12.1 Introduction

Most of the work in the field of polymer crystallization in the last decades has been done on long polymer chains like polyethylene, polypropylene, poly(ethylene oxide) or poly(ethylene terephthalate) which form folded-chain crystals with a typical thickness of about 10 nm [1–5]. In all these cases chain folding plays an important role and crystallization starts from a chemically homogeneous melt. More recently, the confined crystallization of polymers in small domains of microphase-separated block copolymers has attracted a lot

E. Hempel et al.: *Crystallization of Frustrated Alkyl Groups in Polymeric Systems Containing Octadecylmethacrylate*, Lect. Notes Phys. **714**, 201–228 (2007)
DOI 10.1007/3-540-47307-6_12

of attention [6, 7]. The influence of constraints on the crystallization behavior of main chain polymers has been studied in small self-assembled domains with dimensions in the range 10-50 nm. There are different aspects of the crystallization process which can be affected under these conditions. As long as crystallization does not destroy the morphology of the initially microphase-separated block copolymer the influence of confinements on crystal growth and nucleation behavior can be studied [8]. Depending on the morphology the individual crystals can grow only in one (cylinders) or two dimensions (lamellae) [9]. Moreover, a transition from heterogeneous to homogeneous nucleation occurs if the individual compartments are isolated from each other [10, 11]. Nucleation experiments on microphase-separated block copolymers can provide not only average nucleation rates like classical experiments on homogeneous nucleation [12] but also spatially resolved information about the nucleation of individual domains since the crystallizable material is embedded in a solid-like (usually glassy) matrix. Note, that in practically all these cases block copolymers have been used where the crystallizable component is a main chain polymer. Thus, long chains must reorganize in small domains before crystallization can take place. Although there is an incredible number of experimental results and various theoretical approaches basic aspects of the polymer crystallization are still not finally understood. Details of nucleation mechanism and early stages of crystallization [13, 14] are not yet clear and even the question whether the crystal thickness is determined by equilibrium thermodynamics or a consequence of non-equilibrium effects is controversially debated [15, 16].

Compared to the variety of studies on crystallizable main chain polymers and the accumulated phenomenological knowledge about their crystallization behavior relatively less is known about the crystallization of side chain polymers. Only some studies reporting details on the side chain crystallization process can be found in the literature [17–21] although polymers with long alkyl groups in the side chain are studied since the early days of polymer research [22]. Recent experiments on amorphous side chain polymers like methacrylates [23, 24], acrylates [24], itaconates [17, 25] or hairy rod polyimides [26] have shown that there is a nanophase separation of main and side chain parts already in the melt. Long alkyl groups belonging to different monomeric units aggregate in alkyl nanodomains with a typical size in the range 0.5-2 nm [24]. If the alkyl groups are long and flexible enough side chain crystallization can occur [27]. In contrast to the situation in main chain polymers the crystallization process in these side chain polymers starts from a nanostructured melt. The confined side chain crystallization process in microphase-separated block copolymers has not been investigated in great detail so far. Some studies which are more focused on the structure of block copolymers containing liquid-crystalline side chain polymers have been presented recently [28–31]. The results indicate that block copolymers with one component being a side chain polymer are interesting materials which show potentially a hierarchy of length scales in the nanometer range. It seems to

be interesting to see to which extent side chain crystallization and nanophase separation are affected by the concurrence of two length scales in the nanometer range in microphase-separated block copolymers with a crystallizable side chain polymer as one component.

The following chapter deals with the side chain crystallization process in poly(n-octadecylmethacrylate) homopolymers [PODMA] with $C = 18$ alkyl carbon per side chain as well as microphase-separated poly(styrene−*b*−octadecylmethacrylate) block copolymers [P(S−*b*−ODMA)] containing lamellar and cylindrical PODMA domains. Results from calorimetric measurements and X-ray as well as synchrotron scattering data will be presented. The chapter is divided in two sections: The first part is related to the crystallization behavior PODMA homopolymers with different molecular weight. The influence of immobile main chains on the crystallization of long frustrated alkyl groups aggregated in alkyl nanodomains with a typical dimension of about 2 nm will be discussed. A four stage picture for the crystallization of frustrated alkyl groups is proposed. The second part deals with the confined side chain crystallization in small (10-25 nm) PODMA domains of microphase-separated P(S−*b*−ODMA) block copolymers. The influence of constraints introduced by the glassy polystyrene phase on the crystallization kinetics is shown. Changes concerning crystal growth, nucleation behavior and degree of crystallinity are discussed and speculative pictures for the internal structure of lamellar and cylindrical PODMA domains are considered.

12.2 Side-chain Crystallization in Poly(*n*-octadecylmethacrylate)

Higher poly(*n*-alkyl methacrylates) have been studied since the early 1950s by various experimental techniques like dilatometry, x-ray scattering, calorimetry, dielectrics and shear spectroscopy [32–36]. Most of the studies deal with relaxation behavior and properties of amorphous members although it was already known at that time that the alkyl groups in the side chains can crystallize if they are sufficiently long. Atactic poly(n-alkyl methacrylates) with $C \geq 12$ alkyl carbons per side chain are able to crystallize. About further details of the side chain crystallization in poly(n-alkyl methacrylates), however, is still not too much known. There are only a few papers in the literature which are focused on this topic [19, 37]. Otherwise, higher poly(n-alkyl methacrylates) belong to the interesting class of materials where long CH_2 sequences can crystallize with the specialty that the microstructure restricts crystallization to sequences with a finite length.

Crystalline systems containing long sequences of CH_2 units are of extraordinary importance in many fields. *Polyethylene* is the mostly used polymer with a variety of technical applications but has a lot of unusual features which are not completely understood. Peculiarities are the large mobility of

chain segments in the crystalline state, significantly thickening of the crystals during the crystallization process [38], a transition from orthorhombic to hexagonal packing in "defected" polyethylenes [39] or the occurrence of shish-kebab structures in polyethylene blends crystallized under shear [40,41]. *Linear alkanes* with 10 to 25 carbons are basic ingredients of petroleum and have been studied in any detail [12, 42–45]. Also these molecules show peculiarities namely the occurrence of hexagonally packed mesophases – so called rotator phases – in a narrow temperature interval between liquid and orthorhombic phase [43, 46, 47] and surface induced crystallization at the liquid-to-rotator transition [48, 49]. *Phospholipids* consisting of a hydrophilic head group and long hydrophobic alkyl groups are a third class of materials where alkyl sequences can crystallize in several modifications. Various membranes and vesicles in biological systems are designed by nature based on phospholipids. Somehow the crystallization in side chain polymers with long alkyl groups can be seen as a crystallization of alkanes in the presence of external constraints. Similarities to the situation of short polyethylene sequences stretched between two entanglements are obvious. Interestingly some of the typical features of polyethylene and alkanes seem to survive in crystallizable side chain polymers with long alkyl groups. This may indicate that the crystallization behavior of alkyl groups is modified but not completely changed if they are frustrated since they are bonded to a main chain with lower mobility. Thus, we believe that studies on side chain polymers with long alkyl groups are not only important to understand the crystallization behavior of these systems but may also contribute to a better understanding of peculiarities in other system containing long CH_2 sequences.

In the recent years it has been shown based on x-ray scattering and relaxation spectroscopy data for a series of atactic poly(n-alkyl methacrylates) series that long alkyl groups belonging to different monomeric units and chains aggregate in the melt [23, 24, 50]. Small alkyl nanodomains with a typical dimension in the range 0.5–2 nm are formed in systems with $C = 4$ to $C = 18$ alkyl carbons per side chain. Depending on the length of the alkyl groups or equivalently the size of the alkyl nanodomains the CH_2 units either remain disordered for $C < 12$ and show an independent dynamics in form of a "polyethylene-like glass transition" reflecting the independence of the dynamics of the alkyl groups [24] or undergo for $C > 12$ a crystallization process [32, 51]. The transition between both situation is interesting because early stages of crystallization might be stabilized due to frustration of the alkyl groups by the immobile main chains. In the following part results for the side chain crystallization in poly($n-$octadecylmethacrylate) with $C = 18$ alkyl carbons per side chain will be presented. Atactic PODMA samples with different molecular weights synthesized by anionic polymerization are investigated (Table 12.1).

Scattering data for high molecular weight PODMAs in the molten state show a relatively broad prepeak with a maximum at $q \approx 2.1$ nm^{-1} (Fig. 12.1). According to a Bragg approximation this peak corresponds to a distance

Table 12.1. Characterization of the PODMA homopolymers and parameters describing the crystallization process

Sample*	M_n	M_w/M_n	D_c	$T_m^{max\dagger}$	$T_c^{max\dagger}$	$u^{\#}$	$n^{\ddagger}$
	kg/mol		mol%	°C	°C	10^{-3}	
ODMA8	2.8	2.3	29	33	23	34 (23)	4.5
ODMA16	5.3	1.8	30	34	24	34	4.0
ODMA27	9.0	2.1	31	32	25	34 (26)	4.1
ODMA53	18.1	1.5	28	33	23	34 (24)	3.7
ODMA88	29.8	1.8	27	34	24	34	3.4
ODMA100	33.7	1.8	29	35	25	34	3.5

* The numbers give the degree of polymerization P. † Peak maxima from scans with rates of ±10 K/min. # Taken from scans with rates of ±10 K/min (±1 K/min). ‡ Taken from Avrami plots (cf. Fig. 12.12). The uncertainty is about ±0.2. The width of the transformation interval can be estimated according to $\Delta \log t_c = 1.253/n$ (cf. [37]).

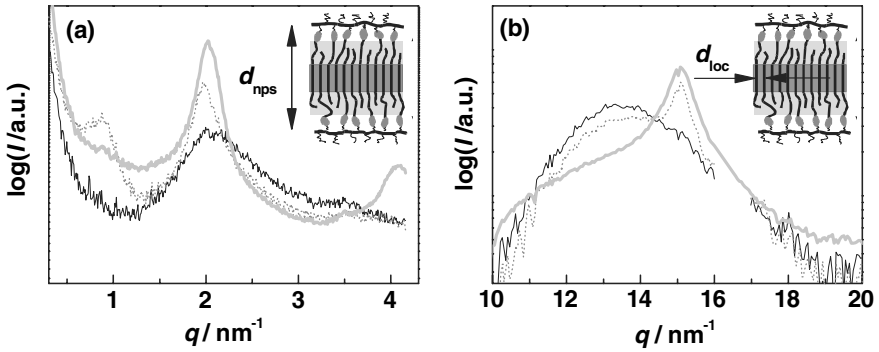

Fig. 12.1. Small (**a**) and wide (**b**) angle scattering data for PODMA27 in the amorphous state (*thin lines*) and two semi-crystalline (*dotted and thick lines*) states measured simultaneously on beam line BM26 at the ESRF in Grenoble. The amorphous state corresponds to a sample which is measured 1min after a quench from 50 to 25°C. The semi-crystalline samples are crystallized at room temperature for 2min (*dotted*) or more than one week (*thick*). Schematic pictures of the structure of semi-crystalline PODMA are shown in the insets (*small ellipses*: carboxyl groups; *light gray*: alkyl nanodomains; *dark gray*: crystalline layer). The length scales d_{nps} and d_{loc} corresponding to the scattering peaks in the small and wide angle ranges are indicated (further details see text)

of about $d_{nps} = 2\pi/q_{\max} \approx 2.9$ nm. During the side chain crystallization process the prepeak sharpens and shifts slightly to smaller q values. The peak maximum for the semi-crystalline PODMA samples occurs at $q \approx 2$ nm^{-1} corresponding to $d_{nps} \approx 3.1$ nm. The reduced peak width indicates an increase of the correlation length. The occurrence of a prepeak shows that the

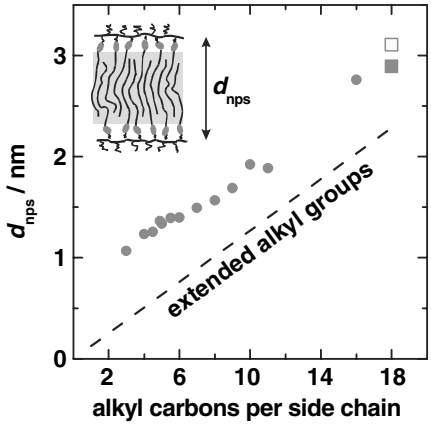

Fig. 12.2. Equivalent Bragg spacing d_{nps} as calculated from the maxima of the pre-peaks for lower amorphous poly(n-alkyl methacrylates) (•) as well as amorphous (■) and semi-crystalline (□) PODMA (cf. Fig. 12.1). The inset shows a schematic picture of the structure of amorphous poly(n-alkyl methacrylates)

crystallization of long alkyl groups in PODMA starts from a pre-structured melt. Long alkyl groups belonging to different monomeric units and chains aggregate already in the melt like in lower poly(n-alkyl methacrylates) where the side chains are unable to crystallize. In PODMA a higher order peak at $q \approx 4.1$ nm^{-1} appears after sufficiently long crystallization under ambient conditions. This indicates lamellar packing, i.e. small stacks formed by alternating layers with high main chain or high side chain concentration. Note, that the scattering contrast in PODMA is basically due to differences in the electron density between carboxyl groups and alkyl nanodomains. Thus, nanophase separation can be already seen in the melt. The prepeak reflects basically the main chain to main chain distance. This situation is only modified during the crystallization process due to an increase of the electron density in the crystalline parts of the alkyl nanodomains. Thus, further details like the thickness of the crystalline layers can not be extracted from x-ray scattering data easily.

A schematic picture of the structure of semi-crystalline PODMA is shown in the insets of Fig. 12.1. Basic idea is that the alkyl groups belonging to different monomeric units form layer-like alkyl nanodomains which are separated by main chains. The periodicity d_{nps} of this lamellar structure reflected by the prepeak in x-ray scattering data is indicated. We assume that the alkyl groups within the alkyl nanodomains are basically interdigitated and not to far away from an extended chain conformation. This can be concluded from the dependence of the d_{nps} value on the number of alkyl carbons per side chain C for atactic poly(n-alkyl methacrylates) (Fig. 12.2). The dependence of d_{nps} on C is nearly linear and the slope is about 0.13 nm [50] per additional CH_2 unit in the side chain corresponding to the value reported for extended chain alkanes (0.127 nm/carbon).

The halo in the scattering data for amorphous PODMA around $q = 13.5$ nm^{-1} reflects the average distance between non-bonded alkyl carbons in the melt ($d_{loc} = 0.465$ nm). During crystallization a sharp reflex at $q \approx 15.1$ nm^{-1} develops on top of the amorphous halo. This corresponds

to a d_{loc} value of about 0.41 nm which is expectedly significantly smaller than for the amorphous sample. The absence of additional peaks for the semi-crystalline sample shows that the crystalline alkyl segments are hexagonally packed. This corresponds to the situation in the rotator phase of alkanes [43,46,47] or in strongly defected polyethylenes [39]. The reduced average distance in the crystalline state is related to the increase in the average density during crystallization ($\Delta\rho \approx 4.5\%$ [32]). Note, that the d_{nps} value increases while the d_{loc} decreases during the crystallization. This indicates that the densification process is highly anisotropic on a molecular scale. The small increase in the main chain to main chain distance d_{nps} during crystallization can be explained based on the increasing trans content in the alkyl groups. The most natural assumption seems to be that the crystalline alkyl sequences are located in the middle of the layer-like alkyl nanodomains (cf. insets Fig. 12.1). The nature of an additional peak in the scattering curves at $q \approx 0.95$ nm^{-1} which occurs temporary in the course of the crystallization process is not finally understood. Possibly, this peak indicates a super structure appearing as a transitient state during crystallization. As already mentioned above, the information about structural details in x-ray scattering data is rather limited. Interestingly, more can be learned from DSC experiments.

Isothermal crystallization experiments in the temperature range between 24 and 32°C have been performed using a Perkin Elmer DSC 7 and a Pyris Diamond DSC. The sample with a mass of about 10mg was annealed at $T = 50$°C significantly above the melting temperature for ten minutes, quenched with a rate of –40 K/min to the crystallization temperature T_c, isothermally crystallized for a given time t_c and finally reheated with a rate of +10 K/min. The melting peak in the heating scans contains the information about the crystalline material formed during isothermal crystallization. A representative set of heating curves measured after isothermal crystallization at $T_c = 31.5$°C is shown in Fig. 12.3a. Based on the area of the melting peaks the heat of melting q_m can be determined. In Fig. 12.3b the q_m values are plotted versus crystallization time t_c for different crystallization temperatures T_c. Assuming that the heat of melting for the alkyl groups in PODMA corresponds to that of octadecene ($q_{m,OD} = 61.4$kJ/mol [37]) one can estimate the degree of crystallinity of the alkyl groups according to $D_c = q_m/q_{m,OD}$. The shape of the different isotherms is quite similar. In all cases a dramatic increase of q_m and D_c is observed in a narrow time interval. This sigmoidal increase corresponds to the primary crystallization process and comes to an end at $q_m \approx 45$ J per gram PODMA or analogously at $D_c \approx 25\%$. For larger crystallization times t_c a strong secondary crystallization process is indicated by a linear increase of q_m and D_c on logarithmic time scales. Note, that the secondary crystallization process of PODMA is very pronounced compared to the findings for many other polymers. One should also remember that significant crystal thickening is a special feature of polyethylene.

A clear trend in the isotherms in Fig. 12.3b is that the crystallization kinetics slows down if the crystallization temperature T_c increases. This

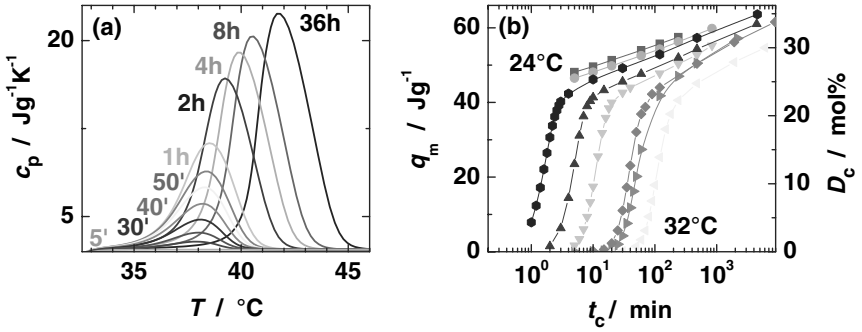

Fig. 12.3. (**a**) DSC heating curves (+10 K/min) for PODMA measured after isothermal crystallization at $T_c = 31.5°$C for different crystallization times t_c. (**b**) Heat of melting q_m and degree of crystallinity D_c vs. logarithm isothermal crystallization time logt_c measured at different temperatures (from the *top* to the *bottom*: $T_c = 24$, 26, 27.7, 29, 30, 31, 31.5, 32°C). The q_m values are calculated from melting peaks as shown in part (**a**) for $T = 31.5°$C

temperature dependence indicates that the crystallization kinetics is dominated by the nucleation process. With decreasing crystallization temperature homogeneous nucleation becomes more and more effective. Obviously, this effect overcompensates the strong decrease in mobility with decreasing temperature. Note, that the strong dependence of the characteristic crystallization time on T_c is accompanied by small undercooling values $u = (T_m - T_c)/T_m$ for PODMA homopolymers obtained from DSC experiments with a rate of ± 10 K/min and ± 1 K/min (cf. Table 12.1). These u values are similar to the values for homogeneously nucleated alkanes in small droplets [42]. Further details of the nucleation behavior will be discussed in the second part of this paper where the crystallization behavior of PODMA homopolymers is compared with findings for microphase-separated P(S−*b*−ODMA) block copolymers.

An interesting detail in Fig. 12.3a is the fact that the peak position is practically time independent for short crystallization times t_c while a significant shift of the peak maximum is observed for longer times. In Fig. 12.4 the melting temperature T_m corresponding to the peak maximum is plotted versus the degree of crystallinity D_c for different crystallization temperatures T_c. This plot shows clearly that the melting temperature T_m is practically constant during the primary crystallization process ($D_c < 25\%$) and that T_m increases systematically in the course of the secondary crystallization ($D_c > 25\%$). This effect occurs for all investigated crystallization temperatures T_c. In the framework in of the Gibbs-Thompson relation ($(T_m^0 - T_m)/T_m^0 \propto 1/L$), where L is the crystal thickness and T_m^0 the melting temperature for a crystal with infinite thickness ($L \to \infty$), this finding indicates that the crystal thickness increases significantly during the secondary crystallization process. According to this picture L is practically constant during the primary crystallization step

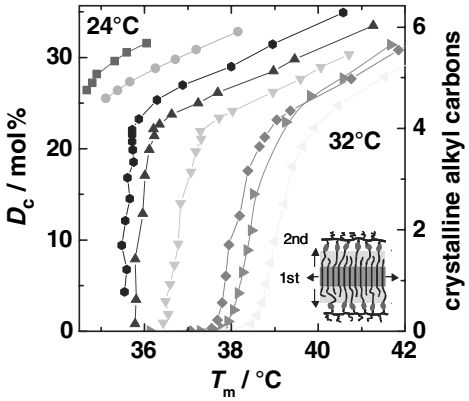

Fig. 12.4. Degree of crystallinity D_c and average number of crystalline alkyl carbons per side chain vs. melting temperature T_m from isothermal crystallization measurements. The symbols correspond to that one used for the different isotherms in Fig. 12.3b. The inset shows schematically the directions of crystal growth during primary (1st) and secondary (2nd) crystallization

although the degree of crystallinity D_c is significantly increasing. Considering a lamellar picture as shown in the inset of Fig.12.4 one can estimate based on the calorimetrically determined D_c values the thickness of crystalline lamellae. From $D_c \approx 25\%$ at the end of the primary crystallization. On gets a stem length of about five alkyl carbons ($L \approx 0.6$ nm).

Calorimetric observations and scattering results presented above allow a relatively detailed description of the side chain crystallization process of long alkyl groups in PODMA homopolymers. We propose a hypothetical picture with four stages: (i) nanophase-separated melt as initial situation for the crystallization of alkyl groups in side chain polymers like PODMA, (ii) nucleation and early stages of crystallization characterized by highly extended alkyl groups, (iii) primary crystallization related to lateral growth of thin crystalline lamellae and (iv) crystal thickening during secondary crystallization. Further details of the different stages are discussed below:

(i) Structural data for amorphous PODMA and other side chain polymers show that long alkyl groups aggregate in the melt. Alkyl nanodomains with a typical size in the range 0.5-2 nm (for PODMA ≈ 2 nm) are formed. Short alkyl groups are frustrated by immobile main chains and unable to crystallize. The dynamics of these amorphous side chain polymers is characterized by an additional polyethylene-like glass transition (α_{PE}) due to cooperative motions within the alkyl nanodomains which are basically decoupled from the main chain dynamics (α). With increasing side chain length frustration effects become less important. If the alkyl groups are long and flexible enough side chain crystallization occurs. Parts of the alkyl groups far away from the main chains are able to reach crystalline order. The length of the alkyl group which is required before crystallization occurs depends on different structural aspects like tacticity but also on the main chain mobility. This can be concluded from a comparison of the crystallization behavior of atactic poly(n-alkyl methacrylates) and poly(n-alkyl acrylates). In case of the poly(n-alkyl acrylates) having more flexible main chains and a significantly lower $T_g(\alpha)$ the octyl member with $C = 8$ alkyl carbons can crystallize while the first methacrylate which

can crystallize is the dodecyl member with $C = 12$ alkyl carbons. All results indicate that the alkyl groups in side chain polymers are already aggregated in the melt before crystallization starts to occur. In order to crystallize the alkyl groups have to overcome frustration introduced by the immobile main chain. This special situation may stabilize states which are unstable or transient and hardly detectable in related systems like alkanes or polyethylene.

(ii) At the transition from the disordered to the crystalline state the alkyl groups in side chain polymers like PODMA are probably in a nearly extended conformation with a large trans content. This is indicated by a nearly linear increase of the main chain to main chain distance d_{nps} for the methacrylate series with a slope of about 0.13 nm per additional CH_2 unit similar to the values reported for crystalline alkanes (Fig. 12.2). Another argument supporting this idea is the fact that d_{nps} is only slightly changing during crystallization. The occurrence of highly extended alkyl groups in the amorphous state might be related to some of the unusual features observed for different systems containing long CH_2 sequences. It has been discussed recently that highly stretched chain segments act as nucleation sites in sheared polyethylene blends [13, 40, 52, 53]. Low molecular weight PEs mixed with a small fraction of ultra-long PE chains show this phenomenon quite clearly [41, 54]. Based on these similarities one can speculate that the nucleation mechanism for side chain polymers with alkyl groups is similar. Whether or not this is a more general mechanism for polymeric systems containing long alkyl sequences remains open. The fact that most of these systems show small undercooling and the occurrence of hexagonally packed (meso)phases is at least remarkable.

(iii) Once the primary crystallization has started the degree of crystallinity D_c increases rapidly. Calorimetric results indicate that thin crystalline lamellae with a constant thickness of about 0.6 nm corresponding to a stem length of about five carbons grow laterally within existing alkyl nanodomains (inset Fig. 12.4). This can be concluded from the constant melting temperature during the primary crystallization based on the Gibbs-Thompson relation. The general arrangement of the alkyl groups is obviously unaffected by the crystallization process. The alkyl groups are interdigitated before and after crystallization has taken place. The small increase in the main chain to main chain distance d_{nps} from 2.9 nm to 3.1 nm can be understood as a direct consequence of the increasing trans content in the alkyl groups during crystallization. The most natural assumption is that the crystalline lamellae are located in the middle of the alkyl nanodomains where the constraints introduced by the immobile main chains are minimal. It is an open question so far whether or not the side chain crystallization in atactic PODMAs requires rearrangements on larger scales. This point needs further investigation. Note, that there is a additional peak in the scattering curves at $q \approx 0.95\ \mathrm{nm}^{-1}$. This peak disappears (or can not be resolved) if crystallization has reached some perfection. The nature of this peak is not finally understood but it might be an indication for the existence of a (temporary) super structure.

(iv) The secondary crystallization in PODMA seems to be related to a thickening of the thin crystalline lamellae in the alkyl nanodomains, i.e. the crystal grows in direction which is basically perpendicular to the direction of growth during primary crystallization (inset Fig. 12.4). This is concluded from the significant increase of melting temperature T_m with the degree of crystallization D_c on logarithmic time scales under isothermal conditions. This effect is observed for all investigated temperatures. Crystal thickening is related to a transition of CH_2 units from the non-crystalline part of the alkyl groups to the hexagonally packed crystal. According to the simple lamellar picture shown in the inset of Fig. 12.4 secondary crystallization should come to an end if the thickness of the crystals approaches the length of the alkyl groups. However, the degree of crystallization D_c in our isothermal crystallization experiments on PODMA was always much smaller than 100%. Secondary crystallization starts at $D_c \approx 25\%$ and the largest D_c value reached in our calorimetric studies after long isothermal crystallization times was $D_c \approx 35\%$. This corresponds to a change in the stem length from nearly five to a bit more than six alkyl carbons. In the framework of our picture this means that there are still six alkyl carbons in the amorphous spacers between the crystalline layer in the center of the alkyl nanodomain and the immobile methacrylate main chains. Studies of the saturation process might be interesting in order to understand details of the interrelation between crystallization tendency of the frustrated alkyl groups and mobility of the main chains.

An additional result of this study is that the crystallization behavior of PODMA is practically independent on the molecular weight of the sample. The overall crystallization behavior with a strongly temperature dependent primary crystallization and a pronounced secondary crystallization process is nearly unaffected in PODMA samples with degrees of polymerization in the range $6 < P < 100$. All parameters describing the primary crystallization process like temperature-dependent crystallization time, degree of crystallinity and width of the transformation interval are very similar for all investigated samples (Table 12.1, [27]). This observation is consistent with a relatively robust structure of the nanophase-separated melt which is also observed for amorphous poly(n-butyl methacrylate) samples with different degree of polymerization ($6 < P < 1000$) [55] and the observation that the dynamics within the disordered alkyl nanodomains is basically decoupled from that of the main chain in several series of side chain polymers. Thus, we expect that the proposed picture for the crystallization of frustrated alkyl groups might be applicable to various side chain polymers containing long alkyl groups.

12.3 Confined Crystallization in Microphase-separated Poly(styrene−*block*−octadecylmethacrylate) Copolymers

An interesting approach to learn more about polymer crystallization in general and about the influence of constraints on the crystallization in nanostructured systems in detail are experiments on microphase-separated block copolymers with crystallizable component. This idea has been applied to various block copolymers with long main chain polymers like polyethylene, poly(ethylene oxide) or poly(ϵ−caprolactone) as crystallizable component. In most of the studies the confining component was amorphous but the mobility has been varied in a wide range. The amorphous component can be either glassy or rubbery during the crystallization of the second component. The situation is called "strong confinement" case if the block copolymer morphology is not affected by the crystallization process [8]. This is the typical situation for systems where the glass temperature T_g of the amorphous block is significantly higher than the crystallization temperature T_c of the crystallizable block. Such systems have been used in the last decades to study details of nucleation behavior and crystal growth. Strong confinement situations have been also observed in strongly segregated block copolymers having a amorphous component which is rubbery during the crystallization ($T_g \leq T_c$). The other extreme – called "breakout behavior" [8] – is characterized by the dominance of the crystalline structure and the disappearance of the original block copolymer morphology in the semi-crystalline state. Breakout behavior is typically observed in weakly segregated block copolymers with an amorphous component which is rubbery during the crystallization [56, 57].

Polymer crystallization in strong confinement has been studied frequently but the confined crystallization in block copolymers containing crystallizable side chain polymers has not been studied in much detail so far. An interesting question is whether or not confinement effects on the crystallization behavior are similar to those in previously studied systems where long main chains do crystallize. As discussed in the previous section (12.2) semi-crystalline side chain polymers are characterized by a lamellar packing of alkyl nanodomains and main chains. The periodicity of this basically lamellar structure depends on the length of the alkyl groups and is reflected by the prepeak in x-ray data. Thus, block copolymers containing side chain polymers as crystallizable component are potentially systems with a hierarchy of length scales in the nanometer range. Two coexisting structural elements are expected: One is due to the microphase-separation of the two blocks (10-50 nm) and a second scale is due to the nanophase-separation of the side chain polymer (2-3 nm). The interrelation between these two length scales in microphase-separated block copolymers with one component being a crystallizable side chain polymer is another interesting phenomenon in these systems. Whether or not both structures survive in these complex systems is not a priori clear because two mechanisms of structure formation concur. According to the picture for the

Table 12.2. Characterization of the P(S-*b*−ODMA) block copolymers and parameters of the crystallization process

Label*	Φ_{ODMA}	N_{ODMA}	N_S	M_w/M_n	D_c	$T_c^{max\dagger}$	$T_m^{max\dagger}$	T_ω^+	$u^\#$	$n^\ddagger$
					mol%	°C	°C	°C	10^{-3}	
Lam-9 nm	0.39	25	154	1.1	25	20.4	32.4	94	39 (31)	2.8
Lam-17 nm	0.44	52	257	1.1	27	22.8	33.8	102	36 (32)	3.4
Cyl-11 nm	0.18	12	224	1.1	15	8.7	17.7	94	31 (24)	0.7
Cyl-16 nm	0.16	21	448	1.1	30	18.3	31.1	103	42 (-)	1.5
Cyl-24 nm	0.26	38	426	1.1	30	20.6	33.3	103	41 (-)	1.8
PODMA27	1.00	27	-	2.1	31	23.9	34.3	–	34 (26)	4.1

* The numbers indicate thickness of PODMA lamellae or diameter of PODMA cylinders estimated based on Φ_{ODMA} values from NMR. † Peak maxima from scans with rates of $dT/dt = \pm$ 10 K/min. + Dynamic glass temperatures from c_p''-maxima in TMDSC scans (time period t_p = 60s, temperature amplitude T_a=0.4K, underlying heating rate +2 K/min). # Taken from scans with rates of ±10 K/min (±1 K/min). ‡ Taken from Avrami plots (Fig. 12.12). The uncertainty is about ±0.2. The width of the transformation interval can be estimated from $\Delta \log t_c = 1.253/n$ (cf. [37]).

side chain crystallization presented in Sect. 12.2 nanophase separation and side chain crystallization are strongly related phenomena.

In the following part we present detailed experiments on microphase-separated poly(styrene−*b*−octadecylmethacrylate) block copolymers [P(S−*b*−ODMA] containing PODMA domains with a typical size of 10-25 nm (Table 12.2). Structural aspects of these systems are studied by scattering techniques in different q ranges. It will be shown that nanophase separation still occurs and that long alkyl groups can also crystallize in small PODMA domains. The influence of confinement on different aspects of the crystallization behavior like crystallization kinetics, nucleation mechanism, and degree of crystallinity is studied by calorimetry and scattering techniques.

Scattering data for two representative P(S−*b*−ODMA) block copolymers from synchrotron scattering experiments on beam line BM26 at the ESRF in Grenoble are shown in Fig. 12.5. All block copolymers in this study are annealed in a first step at 150°C for 24h under vacuum in order to prepare microphase-separated samples. The curve in Fig. 12.5a for a P(S−*b*−ODMA) block copolymer containing 39*vol*% ODMA (Lam-9 nm) shows typical features of a block copolymer with lamellar morphology while the data in Fig. 12.5b for a sample containing 18*vol*% ODMA (Cyl-11 nm) are consistent with a scattering pattern of a copolymer with cylindrical morphology. Repeating units can be calculated based on maximum position of the first scattering peak $q_{\max}$ and Bragg equation $d = 2\pi/q_{\max}$. By using the ODMA content as obtained from ^{1}H-NMR measurements the size of the PODMA domains was estimated. One gets a thickness of ≈9.5 nm for the PODMA lamellae in the Lam-9 nm sample and a diameter of ≈ 11.5 nm of the PODMA cylinders in the Cyl-11 nm

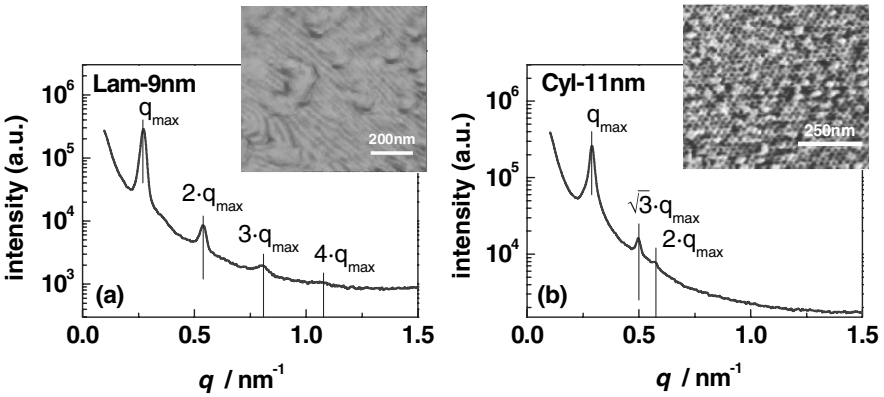

Fig. 12.5. Small angle x-ray scattering data and AFM pictures for microphase-separated P(S-block-ODMA) copolymers with (**a**) lamellar and (**b**) cylindrical morphology. The peak maxima at $q_{\max} = 0.27$ nm^{-1} for Lam-9 nm and $q_{\max} = 0.29$ nm^{-1} for Cyl-11 nm correspond to Bragg spacings of $d_{mps} = 23.3$ nm and $d_{mps} = 21.7$ nm, respectively

sample. Atomic force microscopy (AFM) pictures shown as insets in Fig. 12.5 support the morphologies and domain sizes reported above. Results for several other P(S−*b*−ODMA) copolymers with lamellar and cylindrical morphology will be presented below. The parameters characterizing these samples are summarized in Table 12.2. Further details about the synthesis of the samples by anionic polymerization are discussed elsewhere [37].

DSC heating scans for PS and PODMA homopolymers as well as two P(S−*b*−ODMA) block copolymers (Lam-9 nm, Cyl-11 nm) measured at a rate of +10 K/min after cooling with the same rate (-10 K/min) are presented in Fig. 12.6a. The curves show clearly that the crystallization of PODMA side chains occurs at temperatures far below the glass transition of PS. In the heating scans for the P(S−*b*−ODMA) copolymers the melting peak of PODMA ($T_m \approx 16 - 30$°C) and the glass transition of PS ($T_g \approx 90$°C) coexist. Note, that the melting temperature – defined here based on the maximum of the melting peak – for the PODMA cylinders is smaller than T_m for the homopolymers (Table 12.2). An analysis of the strength of the glass transition in the polystyrene domains shows that Δc_p depends linearly on the weight fraction w_{PS} (Fig. 12.6b). The obtained values are only slightly smaller than the values predicted based on a linear dependence of Δc_p on w_{PS} as determined from ^{1}H-NMR spectra. This confirms that the P(S−*b*−ODMA) block copolymers are microphase-separated and indicates that side chain crystallization occurs in a strong confinement. There should be no significant change of the block copolymer morphology during crystallization since $T_g - T_c$ is large. The dependence of the dynamic glass temperature T_ω from temperature modulated DSC (TMDSC, $t_p = 60$s) on the number of units in the polystyrene block N_S is a bit stronger than predicted by the Fox-Flory equation $T_g \propto 1/N_S$ for the

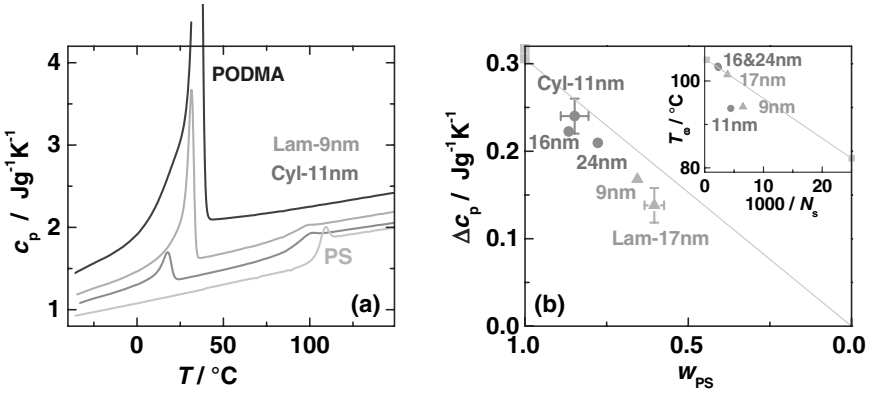

Fig. 12.6. (**a**) DSC heating curves for two P(S−*b*−ODMA) block copolymers with lamellar (Lam-9 nm) and cylindrical (Cyl-11 nm) morphology as well as for PODMA and PS homopolymers. Heating rate was +20 K/min. The curves are measured after cooling with –20 K/min. (**b**) Relaxation strength of the polystyrene phase Δc_p as function of weight fraction PS w_{PS} for five P(S-block-ODMA) copolymers with different morphology. The *dashed line* corresponds to the linear increase of Δc_p with w_{PS}. The inset shows the dynamic glass temperatures T_ω from TMDSC ($t_p = 60$s) depending on the reciprocal number of styrene units is the PS block. The *dotted line* is an interpolation between the T_ω values for two PS homopolymers with different molecular weights based on the Fox-Flory-equation

homopolymer. Similar behavior is reported for several block copolymers and might be due to small differences in chain conformation as well as average density compared to the bulk situation.

Information about internal structure of the PODMA domains and influence of the confinement on the nanophase separation in side chain polymers can be obtained from scattering data for microphase-separated P(S−*b*−ODMA) block copolymers in a wide q range. Experiments on beam line BM26 at the ESRF are an extraordinary way to perform simultaneous online measurements in the small and wide angle range on one sample. Results for our block copolymers indicate that these samples are indeed systems with a hierarchy of length scale in the nanometer range. Representative data for a sample with lamellar morphology (Lam-17 nm) are shown in Fig. 12.7. In the q range below 1 nm^{-1} (Fig. 12.7a) the typical scattering pattern of a lamellar block copolymer is obtained. Results for the molten and the semi-crystalline state are compared. The scattering curve for the molten sample shows higher order peaks at all integer multiples of $q_{\max}$ while only the odd orders have been detected for the semi-crystalline sample. The fact that position and shape of the first order peak at $q_{\max}$ is unaffected shows nicely that the crystallization occurs in a strong confinement. The disappearance of even orders might be a reflection of density changes during crystallization and is a typical feature of symmetric block copolymers. In the q range between 1 nm^{-1} and 4 nm^{-1} the prepeak

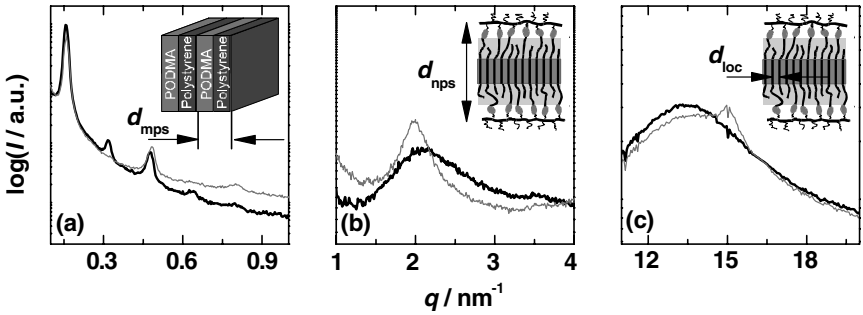

Fig. 12.7. Scattering curves for a lamellar P(S−*b*−ODMA) block copolymer (Lam-17 nm) measured on beam line BM26 at the ESRF in Grenoble (*thick line*: amorphous – $t_c = 1$min, $T_c = 27°$C; thin line: semi-crystalline – $t_c = 20$min, $T_c = 27°$C). Different structural elements are indicated by different scattering peaks: (**a**) microphase separation of PS and PODMA blocks ($d_{mps} \approx 40$ nm), (**b**) nanophase separation of main and side chains in the PODMA domains ($d_{nps} \approx 3.1$ nm), (**c**) local packing of the alkyl groups ($d_{loc} \approx 0.41$ nm)

of the PODMA is observed. The prepeak reflects basically the main chain to main chain distance in PODMA domains and sharpens during crystallization as discussed above in case of the PODMA homopolymers (cf. Fig. 12.1). Note, that the prepeak positions in lamellar block copolymer and homopolymers are practically identical. This shows that the internal structure of PODMA in lamellae with a thickness of 10-25 nm is comparable to that in bulk PODMA. The scattering data measured in the wide angle range around $q \approx 15$ nm^{-1} (Fig. 12.7c) show that a sharp reflex develops during the side chain crystallization process. The position of this reflex – indicating hexagonally packed alkyl groups – is also comparable to that in PODMA homopolymers. The intensity of the reflex, however, seems to be smaller. This is mainly due to the fact that not only the PODMA component but also the amorphous PS component is contributing to the amorphous halo. Moreover, the isothermal crystallization time in this experiment was relatively short (20min at 27°C) resulting in a degree of crystallinity which is significantly smaller compared to the situation for the homopolymer shown in Fig. 12.1 ($t_c >1$ week at $T_c \approx 25°$C).

A more detailed interpretation of the internal structure of the PODMA domains is possible based on WAXS data for a semi-crystalline block copolymer (Lam-20 nm) measured at room temperature using a Bruker D500 system (Fig. 12.8). Data for polystyrene and semi-crystalline PODMA homopolymers are shown for comparison. It is obvious that the scattering curve for the microphase-separated block copolymer can be interpreted as a superposition of contributions originating from both individual components. The first two peaks (1&2) at $q \approx 2.1$ nm^{-1} and $q \approx 4.3$ nm^{-1} indicate the nanophase separation and the lamellar packing of main and side chains in semi-crystalline

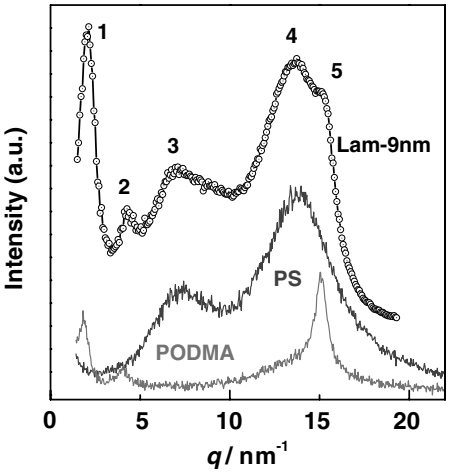

Fig. 12.8. Wide angle scattering curves for a P(S−*b*−ODMA) block copolymer with lamellar morphology (Lam-9 nm) as well as PS and PODMA homopolymers [58]. The curves are shifted vertically. The peak maxima correspond to equivalent Bragg spacings of $d_1 = d_{nps} = 3.05$ nm (second order peak at q_2), $d_3 = 0.85$ nm, $d_4 = 0.46$ nm, and $d_5 = d_{loc} = 0.41$ nm. Further details are discussed in the text

PODMA. The sharp reflex (5) at $q \approx 15.1$ nm^{-1} belongs to the crystalline parts of the alkyl groups in the PODMA domains. The two other peaks (3&4) at $q \approx 7.1$ nm^{-1} and $q \approx 13.7$ nm^{-1} originate mainly from the polystyrene component although a certain part of the amorphous halo (4) is due to non-crystalline CH_2 sequences in the alkyl groups of the PODMA block. The WAXS data support strongly the idea that internal structure and crystallization behavior of PODMA chains in thin lamellae is not influenced by the glassy polystyrene phase in the environment. Note, that this is true for PODMA lamellae with a thickness of about 17 nm as well as those with a thickness of about 9 nm. The structural findings for both samples are quite similar. Interestingly, WAXS data for the cylindrical samples indicate that the nanophase separation in the PODMA domains is surviving also under these more extreme conditions. Although constrained in small cylinders with a diameter of about 10 nm PODMA main and side chains seem to be able to demix on length scales of about 3 nm. All peaks discussed above for the lamellar P(S-b-ODMA) block copolymer have been also found for the samples with cylindrical morphology [59]. The PODMA peaks are less intense due to the volume fraction $0.16 < \phi_{PODMA} < 0.26$ which is significantly smaller compared to the situation in the lamellar samples ($0.39 < \phi_{PODMA} < 0.44$). However, the alkyl groups can crystallize to some extent (Fig. 12.6) and the lamellar order of the individual planes is indicated. Somehow this seems to be surprising since it indicates that both processes of structure formation do not disturb each other too much. Microphase separation in these block copolymers can possibly only occur if the side chain polymers are arranged in an appropriate way within the PODMA cylinders. That alkyl groups belonging to different monomeric units have a strong tendency to aggregate can also be concluded from the fact that random poly(styrene−*stat*−octadecylmethacrylate) copolymers with substantial ODMA content show side chain crystallization [59]. This

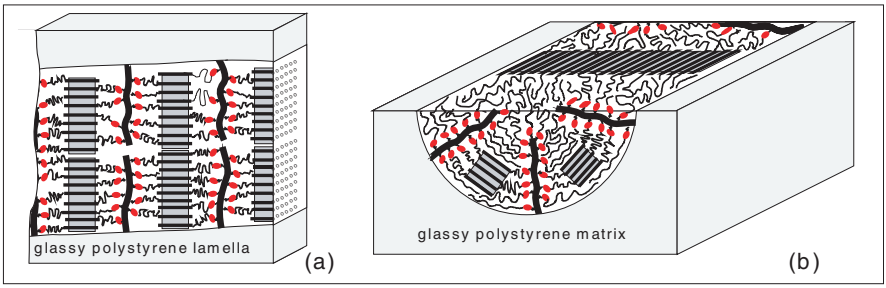

Fig. 12.9. Schematic pictures of the internal structure of the PODMA domains in P(S−*b*−ODMA) copolymers with (**a**) lamellar and (**b**) cylindrical morphology. The small ellipses represent the carboxyl groups of the metharcylate main chains. The dark gray regions are crystalline

can only happen if the alkyl groups are aggregated and tiny alkyl nanodomains are formed.

Hypothetical pictures which may describe the internal structure of PODMA domains in microphase-separated P(S−*b*−ODMA) block copolymers with lamellar and cylindrical morphology are shown in Fig. 12.9. It can be seen that the lamellar morphology fits nicely to the lamellar structure of the nanophases within the semi-crystalline PODMA domains. Thus, confinement effects on the side chain crystallization should not be very pronounced in this case. The main effect might be that the lateral growth of the individual crystalline layers is stopped by glassy polystyrene lamellae. However, the lateral size of the individual crystals in POMDA homopolymers is also limited due to constraints produced by immobile main chains in the environment and it is not clear whether or not the constraints in lamellar block copolymers are really stronger. More pronounced confinement effects are expected for PODMA cylinders since there is a conflict between the curved PS-PODMA interfaces and the basically lamellar structure of semi-crystalline PODMA. Otherwise, nanophase separation seems to be preserved and the side chains can crystallize. A speculative structure which fulfills these requirements is shown in Fig. 12.9b. The main chains are aggregated in certain planes and most of the side chain are oriented parallel to the cylinder axis. Within the main chain planes should be only a limited fraction of alkyl groups which can hardly crystallize. Although the PODMA chains are confined nanophase separation and side chain crystallization can still occur since PODMA forms stacks of main and side chain layers within the cylindrical domains. To which extent side chain crystallization is affected by the environment can not be easily seen in the complex scattering data for microphase-separated P(S−*b*−ODMA) block copolymers. This aspect was studied in more detail by calorimetry.

Isothermal crystallization experiments using DSC support the idea that the crystallization behavior of thin PODMA lamellae in P(S−*b*−ODMA) block copolymers is comparable to that of PODMA homopolymers. The

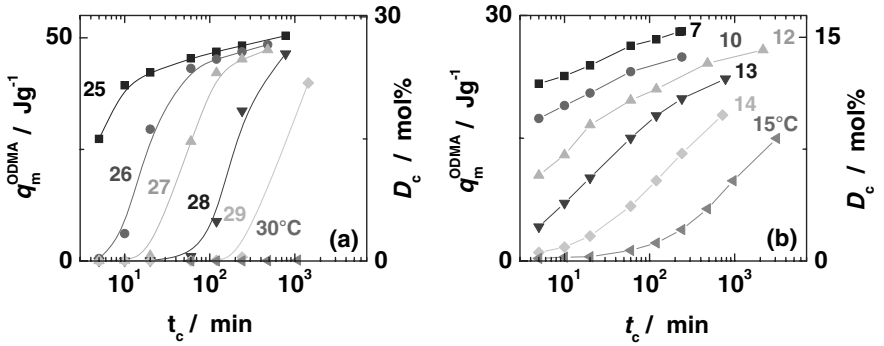

Fig. 12.10. Heat of melting q_m and degree of crystallinity D_c vs. isothermal crystallization time t_c measured at different temperatures for two semi-crystalline block copolymers with (**a**) lamellar (Lam-9 nm) and (**b**) cylindrial (Cyl-11 nm) morphology

applied program is the same which is described in detail in the last Sect. 12.2. The sample is quenched from the melt in the DSC instrument to the isothermal crystallization temperature T_c and hold there for a certain crystallization time t_c. The information about heat of melting per gram ODMA q_m^{ODMA} and degree of crystallinity D_c of the alkyl groups is taken from the melting peak in a subsequent heating scan. The dependence of q_m^{ODMA} and D_c on the isothermal crystallization time t_c is shown for different temperatures in Fig. 12.10a. Obviously, the isotherms for the Lam-9 nm sample are similar to those for the PODMA homopolymer (Fig. 12.3b). Melting temperature, heat of melting per ODMA unit, width of the isothermal transformation interval and overall shape of the isotherms are comparable (Tables 12.1 & 12.2). This can be also seen based on a direct comparison of master curves (Fig. 12.11a) which are constructed from the individual isotherms shown in Fig. 12.10 by a horizontal shift to the isotherm belonging to a certain reference temperature T_{ref}.

A significantly different crystallization behavior is found for small PODMA cylinders with a diameter of about 11 nm in a rigid polystyrene matrix (Cyl-11 nm). The q_m values from isothermal crystallization experiments at different temperatures (Fig. 12.10b) indicate that heat of melting per gram ODMA q_m^{ODMA} and degree of crystallinity are 50% reduced and that the transformation interval is much broader. Compared to homopolymers and lamellar P(S−*b*−ODMA) block copolymers crystallization in small PODMA cylinders occurs at significantly smaller temperatures. A direct comparison of the master curves in Fig. 12.11a shows these differences clearly. Obviously, strong confinement effects occur in case of small PODMA cylinders (Cyl-11 nm) embedded in a glassy polystryrene matrix. The differences in the width of the transformation interval can be also expressed in terms of Avrami coefficients n as obtained from an Avrami plot (Fig. 12.12a) based on the Avrami equation

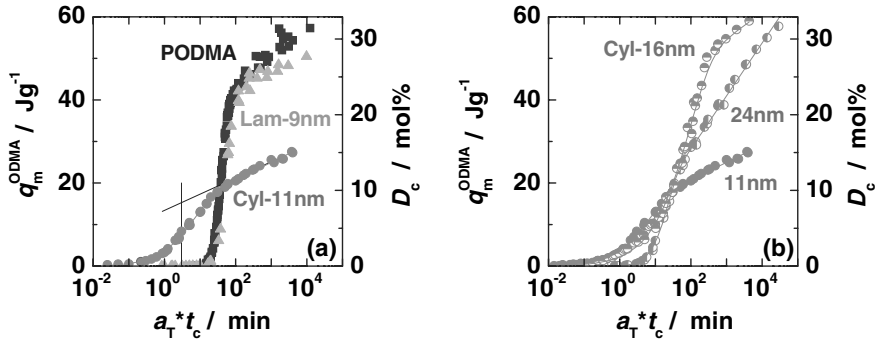

Fig. 12.11. (**a**) Master curves for PODMA27 ($T_{ref} = 31°C$, *squares*) and two semicrystalline P(S−*b*−ODMA) block copolymers with lamellar (Lam-9 nm, $T_{ref} = 27°C$, *triangles*) and cylindrical (Cyl-11 nm, $T_{ref} = 12°C$, *circles*) morphology. The master curves are obtained from isotherms as shown in Figs. 12.3b & 12.10 by a horizontal shift to the given reference temperatures T_{ref}. The tangent construction used to determine the half time $\tau_c(T_{ref})$ is indicated. (**b**) Master curves for three different block copolymers with cylindrical morphology. The diameter of the PODMA cylinders is indicated (Cyl-16 nm, $T_{ref} = 24.2°C$; Cyl-24 nm, $T_{ref} = 26°C$)

$X = 1 - \exp(-kt_c^n)$ with X being the normalized degree of crystalinity and k a rate constant. One gets values $n < 1$ for cylindrical PODMA domains with a diameter of about 11 nm (cf. Table 12.2) while the values for PODMA homopolymers and lamellar block copolymers are in the range $n = 3 - 4$. Note that values $n \approx 0.7$ have been reported for small, homogenously nucleated alkane droplets dispersed in a solvent [12, 42, 45]. Avrami exponents $n = 3 - 4$ have been interpreted as indication for heterogeneous nucleation and three- or two-dimensional crystal growth while $n \approx 1$ indicates homogenous nucleation and/or one-dimensional crystal growth [6, 60].

In a next step the dependence of the confinement effects in cylindrical block copolymers on the diameter of the PODMA cylinders has been checked. Master curves for two systems containing PODMA cylinders with a diameter of 16 nm and 24 nm are compared with those for small 11 nm cylinders in Fig. 12.11b. The data show that there is a strong dependence on the cylinder diameter. The degree of crystallinity D_c which is reached after long crystallization times is higher for the larger diameters. Moreover, there seem to be ranges in the transformation interval with different slopes indicating time- or temperature-dependent changes in the crystallization behavior. A possible explanation for this effect might be the concurrence of heterogeneous and homogeneous nucleation as reported for other crystallizable block copolymer systems [9]. These changes in the curve shape are also reflected in an Avrami plot as shown in Fig. 12.12b. For the largest PODMA cylinders (Cyl-24 nm) the estimated Avrami coefficient is $n \approx 1.8$. This value is already smaller than n for PODMA lamellae and indicates an influence of the confinement. If

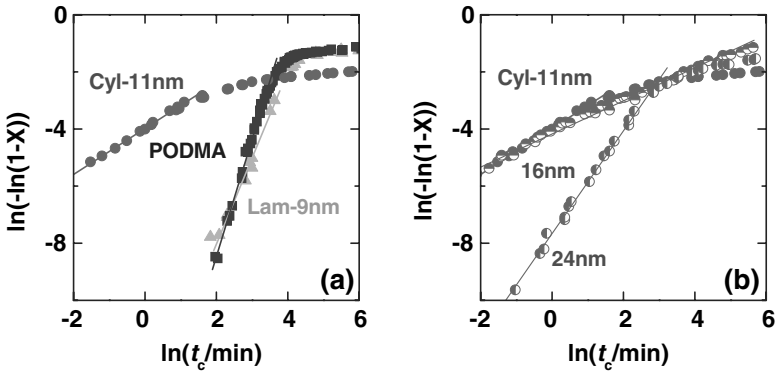

Fig. 12.12. Avrami plots for (**a**) two P(S−*b*−ODMA) block copolymers (Lam-9 nm,Cyl-11 nm) and a PODMA homopolymer and (**b**) block copolymers containing PODMA cylinders with different diameters (Cyl-11 nm,Cyl-16 nm,Cyl-24 nm) constructed based on master curves as shown in Fig. 12.11. Fits to the Avrami equation are indicated by *solid lines*. The fit parameters are given in Table 12.2

the diameter decreases the confinement effects are more pronounced and the n values approach 0.7. This indicates a transition to one-dimensional growth and dominantly homogeneous nucleation. This seems to be in accordance with the intuitive picture that crystals in small cylinders can basically grow only in one direction and that most of the PODMA cylinders are not connected. However, final conclusions about the nature of the changes in the crystallization kinetics under confinement can not be drawn based on Avrami coefficients. Further parameters have to be included in the discussion in order to understand these systems better and to deconvolute changes in nucleation mechanism and crystal growth.

Figure 12.13 shows temperature-dependent half times τ_c as obtained from individual isotherms as shown in Figs. 12.3 & 12.10. The τ_c values are determined using a tangent construction which is shown in Fig. 12.11a and correspond to those crystallization times at which 50% of the primary crystallization at T_c has appeared. A comparison of the $\tau_c(T_c)$ values for different PODMA containing systems shows that the main trends are similar. For all investigated P(S−*b*−ODMA) block copolymers a rapid increase of τ_c with increasing temperature T_c is observed like in the homopolymers. The half times for PODMA lamellae are slightly larger but comparable to those for PODMA homopolymers in the temperature range from 22 to 32°C. In case of block copolymers with cylindrical morphology a strong dependence of τ_c on the diameter of the PODMA cylinders is observed. For the largest diameter (Cyl-24 nm) the crystallization times are similar to those for the smallest lamellae (Lam-9 nm) and only ≈ 30 times larger than the those for the homopolymer. With decreasing diameter of the PODMA cylinders the half time increases dramatically. For the Cyl-16 nm sample τ_c is at least 300 times larger in the

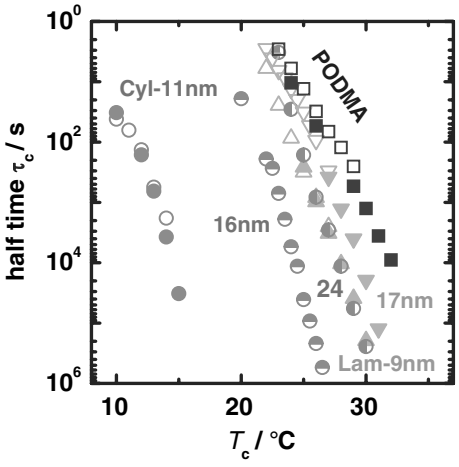

Fig. 12.13. Characteristic crystallization times τ_c vs. crystallization temperature T_c for the homopolymer PODMA27 (*squares*) and block copolymers with lamellar (*triangles*) and cylindrical morphology (*circles*). The curves for different samples are labeled. The *filled and partly-filled symbols* are half times τ_c. The *open symbols* correspond to τ_c values taken from heat flux curves measured during isothermal crystallization (for details see [37])

investigated temperature range while the estimated factor is $> 10^8$ in case of the smallest cylinders (Cyl-11 nm). This trend corresponds to a decrease of the crystallization temperatures in DSC scans measured at constant cooling rate (Table 12.2) and may indicate a transition to homogenous nucleation. Note, that the change in the calorimetrically observed T_c values is significant (T_c(PODMA)$-T_c$(Cyl-11 nm) > 15 K) but relatively small compared to other microphase-separated block copolymers with crystallizable component where the reduction in T_c due to a change from heterogenous to homogenous nucleation is often about 50K [10, 11]. However, the maximal difference in T_c observed for Lam-11 nm copolymer is comparable to the T_c change in case of homogeneously nucleated alkanes. This indicates common aspects in the crystallization behavior although the temperature dependence of the half time τ_c for octadecane is even stronger than that for PODMA [37].

Summarizing the observations above one can conclude that the crystallization behavior of PODMA homopolymers and thin PODMA lamellae surrounded by glassy polystyrene in microphase-separated P(S$-b-$ODMA) block copolymers is basically identical. The temperature-dependent half times $\tau_c(T_c)$, width of the transformation interval (n) as well as degree of crystallinity D_c are similar. There is only a slight increase in the τ_c values accompanied by a small increase in the width of the transformation interval in isothermal crystallization curves reflected by a change from $n \approx 4$ for the homopolymer to $n \approx 3$ for PODMA lamellae. This could be interpreted as a transition from three-dimensional to two-dimensional crystal growth due to constraints in lamellar block copolymers. Dramatic changes in the nucleation mechanism, however, seem to be unlikely. The PODMA lamellae are interconnected and not isolated. The strong decrease of τ_c with decreasing T_c may indicate that homogeneous nucleation is always important in PODMA containing systems. This is somehow consistent with the fact that clear growth

fronts have never been observed in experiments by optical polarization microscopy on PODMA. Seemingly the number of nuclei is always large. The nearly unaffected degree of crystallinity D_c is consistent with the speculative picture for the internal structure of the PODMA lamellae which is shown in Fig. 12.9a. The lamellar structure of semi-crystalline PODMA fits to the lamellar morphology of lamellar P(S−*b*−PODMA) block copolymers. Thus, no significant constraints occur in the interfacial regions which would reduce the degree of crystallinity. According to this picture it is understandable that the D_c values for PODMA lamellae and homopolymers are comparable.

More pronounced confinement effects have been observed in case of P(S−*b*-ODMA) samples containing PODMA cylinders which can crystallize in a glassy polystyrene matrix. The strength of the confinement effects increases if the diameter of the PODMA cylinders decreases: The crystallization kinetics slows down, the width of the transformation interval increases corresponding to a decrease of the Avrami coefficient n and a significant decrease of the D_c values is observed. For the largest cylinders in our series (Cyl-24 nm) the only indication for confinement effects is a significant broadening of the transformation interval corresponding to an Avrami coefficient $n \approx 1.8$ which is much smaller compared to $n \approx 4$ obtained for PODMA homopolymers. Note, that the half times for the Cyl-24 nm and the Lam-9 nm samples are nearly identical. The Avrami coefficient for the Lam-9 nm sample ($n \approx 2.8$), however, is larger than that for the Cyl-24 nm sample. This may indicate that changes in the crystal growth are relevant for the broadening of the transformation interval in case of large cylindrical PODMA domains. With decreasing diameter of the PODMA cylinders the half times increase dramatically and the Avrami coefficient approaches $n \approx 0.7$. This can be explained based on a dominantly homogeneous nucleation process in small cylinders which are basically isolated from each other although a certain fraction of the domains might by interconnected. Thus, heterogeneous and homogeneous nucleation may coexist as discussed for other block copolymers [9]. The reduced degree of crystallinity D_c can be explained based on the speculative picture for the internal structure of cylindrical PODMA domains as shown in Fig. 12.9b. Although the nanophase separation of main and side chains survives inside the cylindrical PODMA domains the D_c values are significantly reduced. The idea is that the alkyl groups close to the main chain planes can not easily crystallize because the curved PS-PODMA interfaces do not fit to the lamellar morphology of semi-crystalline PODMA. Moreover, each imperfection in the position of the main chain in the PS-PODMA interface will lead to a reduced degree of crystallinity D_c since the alkyl groups feel more constraints.

In the light of these results it would be interesting to study the side chain crystallization in well isolated compartments namely in small spherical PODMA domains. Studies of this type have been performed for other block copolymers and give interesting information about the process of homogeneous nucleation [10, 11]. However, we did not succeed so far to prepare microphase-separated P(S−*b*−ODMA) block copolymers containing small

PODMA spheres. One reason might be the complex internal structure of PODMA domains due to the nanophase-separation tendency in this side chain polymer. Possibly there is a strong (possibly irresolvable) conflict between nanophase-separation tendency and formation of PODMA spheres with small diameter. Whether or not there are really peculiarities in the phase behavior of P(S−*b*−ODMA) block copolymers is a topic of further investigations. Work on large molecular weight P(S−*b*−ODMA) samples is in progress. We expect that topological constraints should be less pronounced in case of PODMA spheres with larger diameter since the required curvature of the PS-PODMA interfaces is smaller. Even when PODMA spheres can be formed under these conditions the crystallization tendency of the alkyl groups in spherical PODMA domains should be always severely reduced. However, it is interesting to note in this context that random poly(styrene−*stat*−octadecylmethacrylate) copolymers are able to crystallize. This shows that side chain crystallization of long alkyl groups can occur under extreme conditions and offers interesting opportunities to influence the mechanical properties of polymeric systems systematically [59].

12.4 Conclusions

We have shown in this chapter that the side chain crystallization in poly(n-octadecylmethacrylate) homopolymers can be understood as a crystallization of frustrated alkanes. Due to the fact that long alkyl groups in side chain polymers like higher methacrylates are chemically bonded to a immobile main chain only a certain part of the alkyl groups far away from the main chain is able to reach crystalline order. In PODMA the alkyl groups do crystallize close to room temperature in a hexagonal lattice corresponding to the situation in the rotator phase of alkanes or in highly defected polyethylenes. Scattering data and calorimetric results suggest that the side chain crystallization process in PODMA proceeds in four steps: (i) nanophase separation in the melt = aggregation of alkyl groups belonging to different monomeric units to alkyl nanodomains with a size of about 2 nm; (ii) early stages of crystallization = formation of nuclei in amorphous alkyl nanodomains containing nearly extended alkyl groups; (iii) primary crystallization = lateral growth of a thin layer in the middle of each alkyl nanodomain and (iv) secondary crystallization = thickening of the crystalline layers on logarithmic time scales. Although the situation is surely modified by the existence of immobile main chains several features which are observed in other systems containing long CH_2 sequences seem to be preserved. Otherwise, the constraints may stabilize states which are instable or transient in cases where long CH_2 sequences are less hindered by the environment. This shows that a good understanding of the crystallization process in side chain polymers with long alkyl groups is not only interesting for an understanding of these materials but also for a description of peculiarities in other crystallizable systems.

The results presented in Sect. 12.3 of this chapter demonstrate that microphase-separated poly(styrene−*block*−octadecylmethacrylate) copolymers with lamellar and cylindrical morphology are systems with a hierarchy of length scales in the nanometer range. Self-assembled pattern – formed by classical microphase-separation of incompatible PS and PODMA blocks on a scale of 10–50 nm and due to nanophase separation of main and side chains in the PODMA domains on a scale of 2–3 nm – coexist. Scattering data show in combination with calorimetric results that the crystallization process of PODMA in these systems is a strong confinement case. The polystyrene phase is glassy at those temperatures where side chain crystallization occurs within the PODMA domains. Thus, the crystallization process is unable to change the block copolymer morphology. The influence of constraints introduced by the glassy PS phase on the side chain crystallization in small PODMA lamellae or cylinders was studied in detail by DSC. It is shown that there are only weak confinement effects in case of PODMA lamellae with a thickness of 9–17 nm. The crystallization behavior of the PODMA lamellae is similar to that of PODMA homopolymers. In case of cylindrical POMDA domains the strength of the confinement effects is increasing with decreasing domain size. For large ($d = 24$ nm) cylinders degree of crystallinity D_c and crystallization times τ_c are only slightly affected while for cylinders with a diameter of about 11 nm D_c is 50% reduced and τ_c is $\approx 10^8$ times larger compared to the situation in PODMA homopolymers. The width of the transformation interval during isothermal crystallization is significantly increasing with decreasing diameter, corresponding to a decrease of the Avrami coefficient from $n \approx 1.8$ for the largest ($d = 24$ nm) to $n \approx 0.7$ for the smallest ($d = 11$ nm) cylinders in this study. These results are consistent with a transition from dominantely heterogenous nucleation and three-dimensional crystal growth in bulk PODMA to dominantely homogeneous nuclueation and one-dimensional growth in small cylindrical PODMA domains. The finding that the degree of crystallinity in PODMA lamellae is unaffected while the D_c values in small PODMA cylinders are significantly reduced might be related to the fact that the internally lamellar structure of semi-crystalline PODMA is matching to the lamellar block copolymer morphology while stronger conflicts occur in case of samples with cylindrical morphology. Speculative pictures for the internal structure of the PODMA domains explaining these finding qualitatively have been presented.

In order to quantify the influence of changes in crystal growth and nucleation behavior more seriously experiments on P(S−*b*−ODMA) block copolymers with spherical morphology and definitively isolated PODMA domains would be helpful. The preparation of such materials seems to be a challenge since small PODMA spheres do not form easily. Possibly, there is a conflict between the internal structure of the PODMA domains and the block copolymer morphology if the diameter is too small. However, work along this line is in progress and we are still hopeful that information about nucleation rates can be derived from such systems. Another topic which

has to be settled by additional experiments is the internal structure of the PODMA domains in block copolymers with different morphology. The speculative pictures shown in Fig. 12.9 should be compared with results from scattering experiments on oriented block copolymer samples. In combination with these topics we investigate currently the structure formation in random poly(styrene−*stat*−octadecylmethacrylate) copolymers which show interestingly also side chain crystallization. All these studies on small alkyl nanodomains embedded in a glassy environment should contribute to a better understanding of the nature of early stages of crystallization in case of materials containing long CH_2 sequences.

Acknowledgement

The authors thank Ch. Darko and I. Lieberwirth (Mainz) for assistance with the WAXS measurements, F. Menau and W. Bras (Grenoble) for support at beamline BM26, M. Buschnakowski and S. Henning (Halle) for AFM measurements as well as K. Schröter, Th. Thurn-Albrecht (Halle) and G. Wegner (Mainz) for helpful discussions. This research was supported by German Science Foundation (SFB418) and ESFR Grenoble (SC1779).

References

[1] A. Keller, Phil. Mag. **2**, 1171 (1957).
[2] E.W. Fischer, Z. Naturforschg. **12a**, 753 (1957).
[3] B. Wunderlich, *Macromolecular Physics*. (Academic Press, New York, 1973).
[4] G. Strobl, *The Physics of Polymers*. (Springer, Berlin, 1997).
[5] J.-U. Sommer, G. Reiter, *Polymer Crystallization – Observations, Concepts and Interpretations*. (Springer, Berlin, 2003).
[6] I.W. Hamley, *The Physics of Block Copolymers*. (Oxford University Press, Oxford, 1998).
[7] Y.-L. Loo, and A.J. Ryan, in: I.W. Hamley (ed.) *Developments in Block Copolymer Science and Technology*. (Wiley, New York, 2004).
[8] Y.-L. Loo, R.A. Register, and A.J. Ryan, Macromolecules **35**, 2365 (2002).
[9] Y.-L. Loo, R.A. Register, A.J. Ryan, and G.T. Dee, Macromolecules **34**, 8968 (2001).
[10] G. Reiter, G. Castelein, J.U. Sommer, A. Röttele, and T. Thurn-Albrecht, Phys. Rev. Lett. **87**, 226101 (2001).
[11] Y.-L. Loo, R.A. Register, and A.J. Ryan, Phys. Rev. Lett. **84**, 4120 (2000).
[12] D. Turnbull and R.L. Cormia, J. Chem. Phys. **34**, 820 (1961).
[13] G. Strobl, Eur. Polym. J. E **3**, 165 (2000).
[14] G. Strobl, Eur. Polym. J. E **18**, 295 (2005).
[15] M. Muthukumar, Phil. Trans. R. Soc. Lond. A **361**, 539 (2003).
[16] J.-U. Sommer, *Theoretical Aspects of the Equilibrium State of Chain Crystals*, Lect. Notes in Phys., **714**, 21–45 (Springer, Berlin, 2006).
[17] J.M.G. Cowie, Z. Haq, I.J. McEwen, and J. Velickovic, Polymer **22**, 327 (1981).

[18] J. Clauss, K. Schmidt-Rohr, A. Adam, C. Boeffel, and H.W. Spiess, Macromolecules **20**, 5208 (1992).
[19] M. Mierzwa, G. Floudas, P. Stepanek, and G. Wegner, Phys. Rev. B **62**, 14012 (2000).
[20] G.J.J. Out, A. Turetzkii, and M. Möller, Macromol. Rapid Commun. **16**, 107 (1995).
[21] F. Lopez-Carrasquero et al., Polymer **44**, 4969 (2003).
[22] A. Turner Jones, Macromol. Chem. **71**, 1 (1964).
[23] M. Beiner, K. Schröter, E. Hempel, S. Reissig, and E. Donth, Macromolecules **32**, 6278 (1999).
[24] M. Beiner and H. Huth, Nature Materials **2**, 595 (2003).
[25] V. Arrighi, A. Triolo, I.J. McEwen, P. Holmes, R. Triolo, and H. Amenitsch, Macromolecules **33**, 4989 (2000).
[26] K.W. McCreight, et al., J. Polym. Sci. B: Polym. Phys. **37**, 1633 (1999).
[27] E. Hempel, H. Budde, S. Höring, and M. Beiner, J. Non-cryst. Solids **352**, 5013 (2006).
[28] M. Mao, J. Wang, S.R. Clingman, C.K. Ober, J.T. Chen, and E.L. Thomas, Macromolecules **30**, 2556 (1997).
[29] I.W. Hamley, V. Castelletto, Z.B. Lu, C.T. Imrie, T. Itoh, and A. Al-Hussein, Macromolecules **37**, 4798 (2004).
[30] I.A. Ansari, V. Castelletto, T. Mykhaylyk, I.W. Hamley, Z.B. Lu, T. Itoh, and C.T. Imrie, Macromolecules **36**, 8898 (2003).
[31] O. Ikkala, and G. ten Brinke, Science **295**, 2407 (2002).
[32] S.S. Rogers and L. Mandelkern, J. Phys. Chem. **61**, 985 (1957).
[33] J.D. Ferry *Viscoelastic Properties of Polymers* (Wiley, New York, 1980).
[34] N.G. McCrum, B.E. Read, G. Williams *Anelastic and Dielectric Effects in Polymeric Solids* (Dover Press, New York, 1991).
[35] R.L. Miller, R.F. Boyer, and J. Heijboer, J. Polym. Sci.: Polym. Phys. Ed. **22**, 2021 (1984).
[36] J.L. Gomez Ribelles, M. Monleon Pradas, A. Vidaurre Garayo, F. Romero Colomer, J. Mas Estelles, and J.M. Meseguer Duenas, Macromolecules **28**, 5878 (1995).
[37] E. Hempel, H. Budde, S. Höring, and M. Beiner, Thermochim. Acta **432**, 254 (2005)
[38] M. Hikosaka, K. Amano, S. Rastogi, and A. Keller, J. Mater. Sci. **35**, 5157 (2000).
[39] W. Hu, S. Srinivas, and E.B. Sirota, Macromolecules **35**, 5013 (2002).
[40] P.D. Olmsted, W.C.K. Poon, T.C.B. McLeish, N.J. Terrill, and A.J. Ryan, Phys. Rev. Lett. **81**, 373 (1998).
[41] B.S. Hsiao, L. Yang, R.H. Somani, C.A. Avila-Orta, and L. Zhu, Phys. Rev. Lett. **94**, 117802 (2005)
[42] H. Kraack, E.B. Sirota, and M. Deutsch, J. Chem. Phys. **112**, 6873 (2000).
[43] A.B. Herhold, H.E. King, and E.B. Sirota, J. Chem. Phys. **116**, 9036 (2002).
[44] P. Huber, D. Wallacher, J. Albers, and K. Knorr, Europhys. Lett. **65**, 351 (2004).
[45] R. Montenegro, M. Antonietti, Y. Mastai, and K. Landfester, J. Phys. Chem. B **107**, 5088 (2003).
[46] E.B. Sirota, H.E. King, G.J. Hughes, and W.K. Wan, Phys. Rev. Lett. **68**, 492 (1992)

[47] A.B. Herhold, D. Ertas, A.J. Levine, and H.E. King, Phys. Rev. E **59**, 6946 (1999)
[48] N. Maeda, M.M. Kohonen, and H.K. Christenson, J. Chem. Phys. B **105**, 5906 (2001)
[49] B.M. Ocko, X.Z. Wu, E.B. Sirota, S.K. Sinha, O. Gang, and M. Deutsch, Phys. Rev. E **55**, 3164 (1997)
[50] M. Beiner, Macromol. Rapid Commun. **22**, 869 (2001).
[51] E. Hempel, H. Huth, and M. Beiner, Thermochim. Acta **403**, 105 (2003).
[52] M. Muthukumar, and P. Welch, Polymer **41**, 8833 (2000).
[53] M. Muthukumar, Eur. Polym. J. E **3**, 199 (2000).
[54] L. Yang, R.H. Somani, I. Sics, B.S. Hsiao, R. Kolb, H. Fruitwala, and C. Ong, Macromolecules **37**, 4845 (2004).
[55] S. Hiller, O. Pascui, H. Budde, O. Kabisch, D. Reichert, and M. Beiner, New Journal of Physics **6**, 10 (2004).
[56] R.M. Ho, T.M. Chung, J.C. Tsai, J.C. Kuo, B.S. Hsiao, and I. Sics, Macromol. Rap. Commun. **26**, 107 (2005).
[57] S. Nojima, K. Kato, S. Yamamoto, and T. Ashida, Macromolecules **25**, 2237 (1992).
[58] C. Darko Master Thesis, Universität Halle / MPI-P Mainz (2005).
[59] E. Hempel, H. Budde, S. Höring, and M. Beiner, to be published.
[60] L. Mandelkern, in: J.E. Mark (ed.) *Physical Properties of Polymers*. (Cambridge, Cambridge, 2003).